



Calhoun: The NPS Institutional Archive
DSpace Repository

Theses and Dissertations

1. Thesis and Dissertation Collection, all items

1950

Experimental investigation of detached shock waves on a 70 degree cone at various angles of attack.

Frick, Leo F.

California Institute of Technology

<https://hdl.handle.net/10945/14185>

Downloaded from NPS Archive: Calhoun



Calhoun is the Naval Postgraduate School's public access digital repository for research materials and institutional publications created by the NPS community. Calhoun is named for Professor of Mathematics Guy K. Calhoun, NPS's first appointed -- and published -- scholarly author.

Dudley Knox Library / Naval Postgraduate School
411 Dyer Road / 1 University Circle
Monterey, California USA 93943

<http://www.nps.edu/library>

ALB

GUGGENHEIM AERONAUTICAL LABORATORY

CALIFORNIA INSTITUTE OF TECHNOLOGY

EXPERIMENTAL INVESTIGATION OF DETACHED SHOCK WAVES
ON A 70° CONE AT VARIOUS ANGLES OF ATTACK

Leo F. Frick, LCdr., U.S. Navy

1950

PASADENA, CALIFORNIA

Thesis
F88

Library —
U. S. Naval Postgraduate School
Annapolis, Md.

EXPERIMENTAL INVESTIGATION OF DETACHED SHOCK WAVES
ON A 90° CORNER AT VARIOUS ANGLES OF ATTACK

Thesis by

Lee F. Fritch, Ltjdr., U. S. Navy

In Partial Fulfillment of the Requirements
For the Degree of
Aeronautical Engineer

California Institute of Technology
Pasadena, California

1950

12994

ACKNOWLEDGMENT

The author wishes to express his appreciation to Dr. H. W. Morrison for his continued advice and helpful guidance in the preparation of this thesis and to Miss S. Woodbury for her assistance in the preparation of the manuscript.

This investigation was conducted jointly with Lt. Cdr. William D. Bryan, U. S. Navy.

SUMMARY

An experimental investigation was made to determine the variation of shock shape and extent of subsonic region behind the shock wave with angle of attack for a 70° cone at various Mach numbers. The main interest was centered on those Mach numbers which produced detached shock waves or for which the possibility of detachment at angle of attack existed.

The tests were conducted in the GALCIT 2.5" Supersonic Wind Tunnel at angles of attack of 0° , 3° , 6° , 9° , 12° , and 15° and Mach numbers of 1.458, 1.544, 1.584, 1.957, 1.986, and 3.01.

It was found that, with increasing angle of attack and constant Mach number, the subsonic region behind the shock wave increased in the lower portion and decreased in the upper portion. With increasing Mach number the subsonic region decreased for all angles of attack. Interaction between the upper and lower portions of the shock wave affects the subsonic region behind the wave, suppressing its appearance on the upper surface, retarding its disappearance from the lower surface.

TABLE OF CONTENTS

<u>Part</u>	<u>Title</u>	<u>Page</u>
	Acknowledgements	i
	Abstract	ii
	Table of Contents	iii
	List of Figures	iv
	List of Tables	vi
I.	Introduction	1
II.	Equipment and Procedure	2
III.	Results and Discussion	5
IV.	Conclusions	10
	References	11
	Sample Calculations	12
	Tables	14
	Figures	28

LIST OF FIGURES

<u>Figure No.</u>	<u>Subject</u>	<u>Page</u>
1	Pressure Orifice Location on Models	28
2	Symbols	29
3	Shock Wave Pattern, M = 1.438, Lower	30
4	Shock Wave Pattern, M = 1.438, Upper	31
5	Shock Wave Pattern, M = 1.544, Lower	32
6	Shock Wave Pattern, M = 1.544, Upper	33
7	Shock Wave Pattern, M = 1.534, Lower	34
8	Shock Wave Pattern, M = 1.504, Upper	35
9	Shock Wave Pattern, M = 1.857, Lower	36
10	Shock Wave Pattern, M = 1.857, Upper	37
11	Shock Wave Pattern, M = 1.936, Lower	38
12	Shock Wave Pattern, M = 1.936, Upper	39
13	Shock Wave Pattern, M = 3.01, Lower	40
14	Shock Wave Pattern, M = 3.01, Upper	41
15	Shock Wave Pattern, $\alpha = 0^\circ$, Upper and Lower	42
16	Shock Wave Pattern, $\alpha = 3^\circ$, Lower	43
17	Shock Wave Pattern, $\alpha = 3^\circ$, Upper	44
18	Shock Wave Pattern, $\alpha = 6^\circ$, Lower	45
19	Shock Wave Pattern, $\alpha = 6^\circ$, Upper	46

r

LIST OF FIGURES (continued)

<u>Figure No.</u>	<u>Subject</u>	<u>Page</u>
20	Shock Wave Pattern, $\alpha = 9^\circ$, Lower	47
21	Shock Wave Pattern, $\alpha = 9^\circ$, Upper	48
22	Shock Wave Pattern, $\alpha = 10^\circ$, Lower	49
23	Shock Wave Pattern, $\alpha = 12^\circ$, Upper	50
24	Shock Wave Pattern, $\alpha = 15^\circ$, Lower	51
25	Shock Wave Pattern, $\alpha = 15^\circ$, Upper	52
26	Maximum Flow Deflection (Taylor-Maccoll Theory)	53
27	Surface Pressure Distribution, $M = 1.534$	54
28	Schlieren Picture, $M = 1.534$, $\alpha = 0^\circ$	55
29	Schlieren Picture, $M = 1.534$, $\alpha = 15^\circ$	55
30	Schlieren Picture, $M = 1.534$, $\alpha = 0^\circ$	56
31	Schlieren Picture, $M = 1.534$, $\alpha = 15^\circ$	56
32	Schlieren Picture, $M = 1.957$, $\alpha = 0^\circ$	57
33	Schlieren Picture, $M = 1.957$, $\alpha = 15^\circ$	57

LIST OF CONTENTS

<u>Table No.</u>	<u>Subject</u>	<u>P. c</u>
I.	Tabulation of Mach Number Behind Shock, M = 1.438	14
II.	Tabulation of Mach Number Behind Shock, M = 1.544	17
III.	Tabulation of Mach Number Behind Shock, M = 1.594	20
IV.	Tabulation of Mach Number Behind Shock, M = 1.857	23
V.	Tabulation of Mach Number Behind Shock, M = 1.936	25
VI.	Tabulation of Mach Number Behind Shock, M = 3.01	26
VII.	Condition of Shock	27

1. INTRODUCTION

The theoretical inquiry into the flow around a solid cone at an angle of attack moving with a velocity greater than that of sound, has not advanced to a point where the behavior of the shock waves can be predicted as the cone angle of attack is varied. As a matter of fact, only two cases have so far been found where the motion of a gas at supersonic speed in three-dimensions can, without objectionable simplification be discussed mathematically: the radial outward flow produced by a uniformly expanding sphere; and the flow around a solid cone at zero angle of attack.

Previous investigations, (cf. Ref. 1 and 2), have covered detached shock shapes, pressure distribution on cone surface, and Mach numbers behind the shock for corresponding cones and Mach numbers at zero angle of attack.

The intent of this investigation was to determine experimentally the shape of the shock wave and associated characteristics caused by the presence of a finite cone at various angles of attack in supersonic flow. The detached shocks and those attached shocks, where there was a possibility of detachment occurring at angle of attack, were of primary concern. Also of prime interest was the subsonic flow region behind the shock. One set of pressure measurements at the surface of the cone was taken at a Mach number of 1.584 for angle of attack of zero and twelve degrees.

II. EQUIPMENT AND PROCEDURE

The models used for this investigation were machined from brass, $3/8$ " in diameter and had a cone angle of 70° . Six cone models were used during the course of the investigation, each with a pressure orifice located on the conical surface at varying distances from the nose. A sketch of the cone model with dimensions and location of orifices is shown in Fig. 1. All six cone models were identical except for the location of the pressure orifice.

The investigation was carried out in the GRANT 2.5" Supersonic Wind Tunnel, (Cf. Ref. 3). The model was supported by a sting which could be varied in angle of attack from -5° to $+15^\circ$, but could not be varied in yaw. A flexible nozzle, (Cf. Ref. 1), was used for Mach numbers of 1.438, 1.544, and 1.857. For Mach numbers of 1.834, 2.066, and 3.01 fixed steel nozzle blocks were used. In the case of the flexible nozzle, the nozzle shapes were determined by Puckott's Method, (Cf. Ref. 4).

Calibration of the test section Mach number was accomplished by a static pressure survey along the nozzle centerline in connection with a reference static pressure taken at the test section wall. The centerline survey was made by means of a 0.065" outside diameter tubing with a static orifice. The tubing was fixed with respect to horizontal and vertical movement but was capable of axial movement. In order to

eliminate the measurement of small changes in low pressure, taken along the centerline of the test section, against relatively high atmospheric pressure, the test section centerline static pressure was measured against the reference static pressure. The reference pressure was also measured against atmospheric pressure; then, by subtracting the difference between reference and centerline pressures from the reference pressure, the centerline static pressure was obtained.

The model's zero angle of attack was determined in the following manner. With the model orifice on top, pressure readings were taken at several angles of attack. The model orifice was then switched to the bottom and pressure readings were taken at the same angles of attack. A plot was then made of pressure readings versus angle of attack. Zero angle of attack is given by the intersection of the curves for the orifice on top and the orifice on the bottom.

During all tests the relative humidity of the tunnel was held within .02 to .04 percent by a silica-gel dryer in the tunnel circuit.

Following the calibration of the test section Mach number and model angle of attack the flow field around the model, at angles of attack from 0° to 15° in 5° increments, was photographed by means of schlieren apparatus.

A pressure survey of the cone surface was taken at a Mach number of 1.504 for angles of attack of 0° and 12° , (cf. Fig. 27).

The shock wave patterns in dimensionless form were obtained in the following manner. The negatives of the schlieren photographs were projected on graph paper by means of a photo-enlarger. The photo-enlarger was adjusted so that the diameter of the model was equal to $\pm X/10$ of one on the selected scale, and the shock wave patterns was traced on graph paper. The shock wave patterns for several angles of attack, for one particular Mach number, were superimposed on the same sheet. This procedure was followed for all Mach numbers. The same procedure was also followed in obtaining the shock wave patterns for all Mach numbers at a particular angle of attack. These tracings were used to obtain the final dimensionless curves. By use of this method it was hoped to minimize, in so far as possible, errors associated with transcribing the shock wave patterns to dimensionless coordinates.

2.1. RESULTS OF TESTS

The principal results are presented as dimensionless plots of the shock wave patterns plotted relative to the cone axis rather than to the flow direction. The first series of plots are at constant Mach numbers with angle of attack varying, (Cf. Figs. 8 to 14). The second series are at constant angle of attack with Mach numbers varying, (Cf. Figs. 15 to 25). A third method of presenting the results is a tabulation of the local Mach number directly behind the shock in the subsonic region for each Mach number and angle of attack, (Cf. Tables I to VI). From these tables, the position at which the Mach number behind the shock wave becomes sonic and the position of the normal shock was obtained. This data was indicated on the shock wave plots, where these points were of interest.

A surface pressure survey was taken over both upper and lower cone surfaces at a Mach number of 1.504 for angles of attack of 0° and 12° , (Cf. Fig. 1 and Fig. 27).

Fig. 2 defines the symbols used in the graphical and tabular presentation of the results.

The dimensionless form of the shock wave patterns was obtained by using the cone diameter as the characteristic dimension. Particular attention was given in obtaining the shock wave pattern shape near the nose of the cone; since, in the case of varying angle of attack and

constant Mach number, it was found that some of the shock patterns crossed in this region.

The shock wave patterns for constant Mach number show that close to the nose of the cone the shocks do not have a uniform spread with equal increments in angle of attack; as the vertical distance from the nose of the cone increases the spread becomes regular. It is also clearly shown that with increasing angle of attack the shock wave patterns associated with the upper surface of the cone straighten and assume attached shock characteristics, i.e., no subsonic zone behind shock; while those associated with the lower surface increase in curvature and assume detached characteristics, i.e., a subsonic zone behind shock. This is more clearly brought out by the Mach number curves directly behind the shock.

The variation of shock shapes with Mach number at constant angle of attack are a cross-plot of the previously discussed curves. It is clearly indicated that although the lower portion of the shock waves gradually change their characteristics from attached to detached, those shocks initially attached to the nose of the cone apparently remain attached and those initially detached remain detached.

The Mach number directly behind the shock wave at any point was determined from two-dimensional oblique shock theory by measuring the angle between the shock wave and the flow direction, (cf. Tables I to VI).

At 0° angle of attack the subsonic zone was symmetrical with respect to the cone axis. For increasing angle of attack, at constant Mach number, the subsonic region increased in the lower and decreased in the upper portion of the flow, the rate of decrease being faster than the rate of increase. For constant angle of attack and varying Mach number, the subsonic zone decreases in both the lower and upper portions of the flow.

The Taylor-Maccoll Theory for conical shocks, (cf. Ref. 5), may be used here as a basis of comparison, if it is assumed:

1. That the upper and lower surfaces of the cone may be considered separately.
2. That the angle between the flow direction and the cone surface may be considered as the half-vertex angle of a fictitious cone.

Maximum flow deflection for an initial Mach number, as predicted by the Taylor-Maccoll Theory, is plotted in Fig. 20. The condition of the upper and lower portions of the shock wave for each Mach number is presented in Table VII.

Taking first the lower shock wave pattern at zero angle of attack and increasing Mach numbers, the shock wave has detached characteristics until a Mach number between 1.536 and 1.857 is reached. At some point between these two Mach numbers it assumes attached characteristics. This agreed with the Taylor-Maccoll Theory. The results also agree for

5° angle of attack. At 0° angle of attack corresponding to a half-vertex angle of 42° the Taylor-Maccoll Theory gives as the minimum Mach number for an attached shock wave 1.08. Experimental results indicate a subsonic region in the flow field behind the lower portion of the shock wave at 0° angle of attack for Mach numbers to 1.067. The lower portion of the shock wave at a Mach number of 1.066 does not have a subsonic region; thus, it assumes attached characteristics. A subsonic region, behind the lower portion of the shock wave, for a Mach number of 1.066 does not appear until an angle of attack of 9° is reached. The subsonic region behind the lower portion of the shock wave increase with increasing angle of attack.

For a Mach number of 2.01 the conical shock theory predicts that shock detachment will occur at a half-vertex angle of something less than 50° , corresponding to an angle of attack of less than 15° . However, at an angle of attack of 15° the shock wave still had attached characteristics.

Considering the upper shock, for which this fictitious half-vertex angle can be considered as decreasing with angle of attack, experimental results indicate that the subsonic regions, if initially present, did not disappear for the range of angles of attack investigated. From the conical shock theory at an angle of attack of approximately 0° the shock should become attached for the Mach numbers under consideration.

As a result of the above discussion, it is evident that interaction occurs between the upper and lower portions of the shock wave at an angle of attack. The interaction causes the disappearance of the subsonic region behind the upper shock wave to be delayed and it also delays the disappearance of the supersonic region behind the lower shock wave as the angle of attack is increased.

The pressure measurements for a detached shock, at a Mach number of 1.254, were reduced to the one-dimensional form p_0/p_0' ; p_0' being the reservoir pressure behind the shock wave at the nose of the cone. Pressure measurements were taken on both upper and lower surfaces at 0° and 15° angles of attack.

The plots at constant Mach number and varying angle of attack, for which the shock waves are detached, indicate that the subsonic zone behind the shock wave is decreased with angle of attack.

III. CONCLUSIONS

The following conclusions can be drawn from the results of this investigation:

1. At angle of attack there is a definite interaction between the upper and lower portions of the shock wave.
2. The shock wave if initially attached to the cone remained attached even with the appearance of mixed flow behind the shock, for the range of angles of attack tested.

REFERENCES

1. Hirschner, R. W., and Hitzelner, J., "An Investigation of Detached Shock Waves", Aero. Eng. Thesis, California Institute of Technology, 1948.
2. MacKinnon, W. A., and Muirhead, V. J., "Flow Field Around a Blunt Cone With Shock", Aero. Eng. Thesis, California Institute of Technology, 1949.
3. Puckett, Allen E., and Schanberg, Richard, "Final Report - G-2000 Supersonic Wind Tunnel Tests", Library of Aeronautics, California Institute of Technology, June, 1948.
4. Puckett, Allen E., "Supersonic Missile Design", Journal of Applied Mechanics, December, 1946.
5. Bailey, C. L., and Wood, F. C., "Computation Curves For Compressible Fluid Problems", John Wiley and Sons, Inc., New York, Chapman and Hall, Limited, London.

SAMPLE CALCULATION

A. Determination of Mach number in test section:

 P_{0G} - total reservoir pressure P_1 - reference wall static orifice pressure P_{0C} - static reference pressure P_x - nozzle centerline static orifice pressure.

Density conversion factors:

1 cm. acetylene tetrabromide = .2183 cm. hg.

1 cm. silicone = .0095 cm. hg.

$$\frac{P_x}{P_0} = \frac{P_2}{P_0} - \frac{P_2 - P_x}{P_0}$$

Orifice position	1.0"
P_{0G}	103.0 cm. acetylene tetrabromide
P_a	95.5 cm. acetylene tetrabromide
$P_{0C} - P_a$	2.7 cm. acetylene tetrabromide
.2183 ($P_{0C} - P_a$)	2.12 cm. hg.
Barometer	74.57 cm. hg.
P_0	72.45 cm. hg.
P_a	75.15 cm. hg.
P_{0G}	129.0 cm. hg.
$P_a - P_{2G}$	56.45 cm. hg.
P_2	18.12 cm. hg.

p_2/p_a (av.)	.8437
p_1	69.6 cm. silicone
p_x	64.0 cm. silicone
$p_1 - p_x$	5.6 cm. silicone
.0695 ($p_1 - p_x$)	- .389 cm. hg.
.0695 ($p_1 - p_x$)/ p_0	-.00557
p_x/p_0	.2542
M	1.504

B. Determination of p_0/p_0' , M = 1.504

p_0 = surface pressure on cone

p_0' = reservoir pressure behind normal shock

$$p_0/p_0' = \frac{p_0}{p_0} \approx \frac{p_0}{p_0'}$$

p_0/p_0' was found in the same way as in the determination

of the Mach number.

p_0/p_0	.591
p_0/p_0'	1.109
p_0/p_0'	.535
x'	.2497"
β	.82°
x'/λ	.779

TABLE I

$$\underline{M = 1.433}$$

$\alpha = 0^\circ$		$\alpha = 5^\circ$			
Upper and Lower		Upper		Lower	
Y/D	M_2	Y/D	M_2	Y/D	M_2
0	.750	0	.750	0	.756
.2	.790	.2	.808	.05	.755
.4	.835	.4	.865	.2	.769
.6	.885	.6	.935	.4	.822
.8	.935	.8	.962	.6	.865
1.0	.942	1.0	.990	.8	.900
1.2	.974	1.12	1.000	1.0	.937
1.4	.999			1.2	.958
1.41	1.000			1.4	.991
				1.47	1.000

TABLE 2 (continued)

$$M = 1.438$$

<u>$\alpha = 6^\circ$</u>				<u>$\alpha = 9^\circ$</u>			
Upper		Lower		Upper		Lower	
<u>X/D</u>	<u>M_2</u>	<u>X/D</u>	<u>M_2</u>	<u>X/D</u>	<u>M_2</u>	<u>X/D</u>	<u>M_2</u>
0	.743	0	.743	0	.750	0	.750
.2	.906	.04	.755	.2	.855	.09	.755
.4	.885	.2	.760	.4	.895	.2	.765
.6	.920	.4	.817	.6	.920	.4	.795
.8	.905	.6	.860	.8	.955	.6	.815
1.0	.900	.8	.900	1.0	.900	.8	.880
1.06	1.000	1.0	.954	1.02	1.000	1.0	.860
		1.2	.960			1.2	.900
		1.4	.985			1.4	.940
		1.53	1.000			1.53	1.000

(continued)

$$M = 1.438$$

$\mu = 1.0$				$\mu = 2.0$			
Upper		Lower		Upper		Lower	
Z/σ	Φ	Z/σ	Φ	Z/σ	Φ	Z/σ	Φ
0	.770	0	.770	0	.820	0	.820
.2	.770	.2	.785	.2	.830	.2	.830
.4	.770	.4	.790	.4	.840	.4	.840
.6	.770	.6	.795	.6	.850	.6	.850
.8	.770	.8	.797	.8	.855	.8	.855
.5	1.000	.0	.790	.855	1.000	.0	.790
		1.0	.800	.900		1.0	.800
		1.2	.808	.920		1.2	.808
		1.4	.815	.930		1.4	.815
		1.44	1.000	.940		1.57	1.000

TABLE XI

M = 1.544

<u>$\alpha = 0^\circ$</u>		<u>$\alpha = 90^\circ$</u>			
Upper and Lower		Upper		Lower	
<u>Y/D</u>	<u>M_2</u>	<u>Y/D</u>	<u>M_2</u>	<u>Y/D</u>	<u>M_2</u>
0	.895	0	.700	0	.700
.2	.855	.2	.823	.02	.635
.4	.807	.4	.860	.2	.770
.6	.805	.6	.920	.4	.832
.8	.822	.8	.955	.6	.880
1.0	.870	.98	1.000	.8	.920
1.15	1.000			1.0	.958
				1.17	1.000

TABLE II (continued)

$$M = 1.544$$

$\alpha = 0^\circ$				$\alpha = 9^\circ$			
Upper		Lower		Upper		Lower	
Y/D	M_2	Y/D	M_2	Y/D	M_2	Y/D	M_2
0	.707	0	.707	0	.720	0	.730
.2	.764	.02	.695	.2	.770	.03	.695
.4	.805	.2	.775	.4	.775	.2	.745
.6	.852	.4	.843	.6	.846	.4	.820
.8	.885	.6	.885	.8	.902	.6	.856
1.0	.903	.8	.910	.88	1.000	.8	.900
1.02	1.000	1.0	.960			1.0	.951
		1.12	1.000			1.18	1.000

TABLE II (continued)

$$\underline{M = 1.544}$$

$\alpha = 12^\circ$				$\alpha = 15^\circ$			
Upper		Lower		Upper		Lower	
Y/D	M_2	Y/D	M_2	Y/D	M_2	Y/D	M_2
0	.750	0	.750	0	.740	0	.740
.2	.910	.075	.695	.2	.825	.1	.695
.4	.955	.2	.750	.4	.905	.2	.710
.6	.972	.4	.700	.47	1.000	.4	.770
.68	1.000	.6	.835			.6	.827
		.8	.876			.8	.882
		1.0	.925			1.0	.954
		1.2	1.000			1.2	.990
						1.22	1.000

TABLE III

M = 1.594

<u>$\theta = 0^\circ$</u>		<u>$\theta = 3^\circ$</u>			
Upper and Lower		Upper		Lower	
<u>Z/δ</u>	<u>M_2</u>	<u>Z/δ</u>	<u>M_2</u>	<u>Z/δ</u>	<u>M_2</u>
0	.635	0	.690	0	.690
.2	.907	.2	.912	.02	.685
.4	.912	.4	.952	.2	.915
.6	.925	.6	.960	.4	.920
.8	.949	.8	.990	.6	.918
.96	1.000	.95	1.000	.8	.955
				1.0	.990
				1.06	1.000

TABLE III (continued)

$$M = 1.504$$

$\alpha = 0^\circ$				$\alpha = 9^\circ$			
Upper		Lower		Upper		Lower	
Y/D	M_2	Y/D	M_2	Y/D	M_2	Y/D	M_2
0	.695	0	.695	0	.705	0	.705
.2	.940	.02	.685	.2	.990	.03	.685
.4	.947	.2	.800	.4	.998	.2	.735
.6	.909	.4	.850	.55	1.000	.4	.800
.75	1.00	.6	.858			.6	.846
		.8	.935			.8	.900
		1.0	.990			1.0	.968
		1.055	1.000			1.17	1.000

TABLE III (continued)

N = 1.534

<u>$\alpha = 10^\circ$</u>				<u>$\alpha = 10^\circ$</u>			
Upper		Lower		Upper		Lower	
<u>Y/D</u>	<u>M_2</u>	<u>Y/D</u>	<u>M_2</u>	<u>Y/D</u>	<u>M_2</u>	<u>Y/D</u>	<u>M_2</u>
0	.700	0	.715	0	.720	0	.730
.2	.970	.07	.835	.2	.975	.08	.835
.5	1.000	.2	.752	.25	1.000	.2	.740
		.4	.790			.4	.730
		.6	.837			.6	.800
		.8	.885			.8	.851
		1.0	.953			1.0	.920
		1.16	1.000			1.14	1.000

TABLE IV

$M = 1.857$

<u>$\alpha = 0^\circ$</u>			<u>$\alpha = 3^\circ$</u>		
Upper and Lower			Upper and Lower		
Supersonic			Supersonic		
<u>$\alpha = 0^\circ$</u>			<u>$\alpha = 9^\circ$</u>		
Upper	Lower		Upper	Lower	
	<u>Y/D</u>	<u>M_2</u>		<u>Y/D</u>	<u>M_2</u>
Supersonic	0	.758	Supersonic	0	.880
	.2	.890		.2	.850
	.4	.970		.4	.920
	.6	.995		.6	.970
	.62	1.000		.67	1.000

TABLE IV (continued)

M = 1.857

<u>$\alpha = 12^\circ$</u>			<u>$\alpha = 15^\circ$</u>		
Upper	Lower		Upper	Lower	
	<u>Y/D</u>	<u>M_2</u>		<u>Y/D</u>	<u>M_2</u>
Supersonic	0	.70	Supersonic	0	.625
	.2	.78		.2	.700
	.4	.85		.4	.790
	.6	.93		.6	.867
	.75	1.00		.8	.970
				.85	1.000

TABLE V

M = 1.933

<u>$\alpha = 0^\circ$</u>		<u>$\alpha = 3^\circ$</u>	
Upper and Lower		Upper and Lower	
Supersonic		Supersonic	
<u>$\alpha = 6^\circ$</u>		<u>$\alpha = 9^\circ$</u>	
Upper and Lower		Upper	Lower
Supersonic			Y/D M_2
		Supersonic	0 .960
			.2 .960
			.4 .960
			.6 .972
			.84 1.000
<u>$\alpha = 12^\circ$</u>		<u>$\alpha = 15^\circ$</u>	
Upper	Lower	Upper	Lower
	Y/D M_2		Y/D M_2
Supersonic	0 .850	Supersonic	0 .790
	.2 .860		.2 .810
	.4 .835		.4 .845
	.6 .970		.6 .866
	.88 1.000		.775 1.000

TABLE VI

$$\underline{M = 5.01}$$

Flow was supersonic behind shock
at all angles of attack investigated.

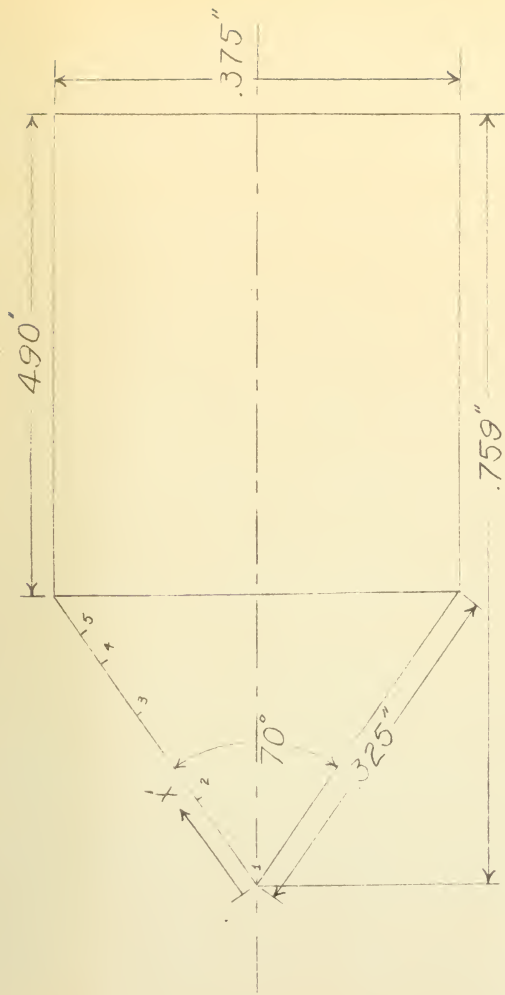
TABLE VII

CONDITION OF SHOCK

		<u>0°</u>	<u>3°</u>	<u>6°</u>	<u>9°</u>	<u>12°</u>	<u>15°</u>
M = 1.488	Upper	D	D	D	D	D	D
	Lower	D	D	D	D	D	D
M = 1.544	Upper	D	D	D	D	D	D
	Lower	D	D	D	D	D	D
M = 1.584	Upper	D	D	D	D	D	D
	Lower	D	D	D	D	D	D
M = 1.657	Upper	A	A	A	A	A	A
	Lower	A	A	D	D	D	D
M = 1.906	Upper	A	A	A	A	A	A
	Lower	A	A	A	D	D	D
M = 3.01	Upper	A	A	A	A	A	A
	Lower	A	A	A	A	A	A

Note: D \curvearrowright detached shock characteristics

A \curvearrowright attached shock characteristics



Case No	X'
1	.000"
2	.097"
3	.193"
4	.250"
5	.284"

FIG. 1
 PRESSURE ORIFICE LOCATION
 ON MODELS
 Scale 8"=1"

FIG. 2
SYMBOLS

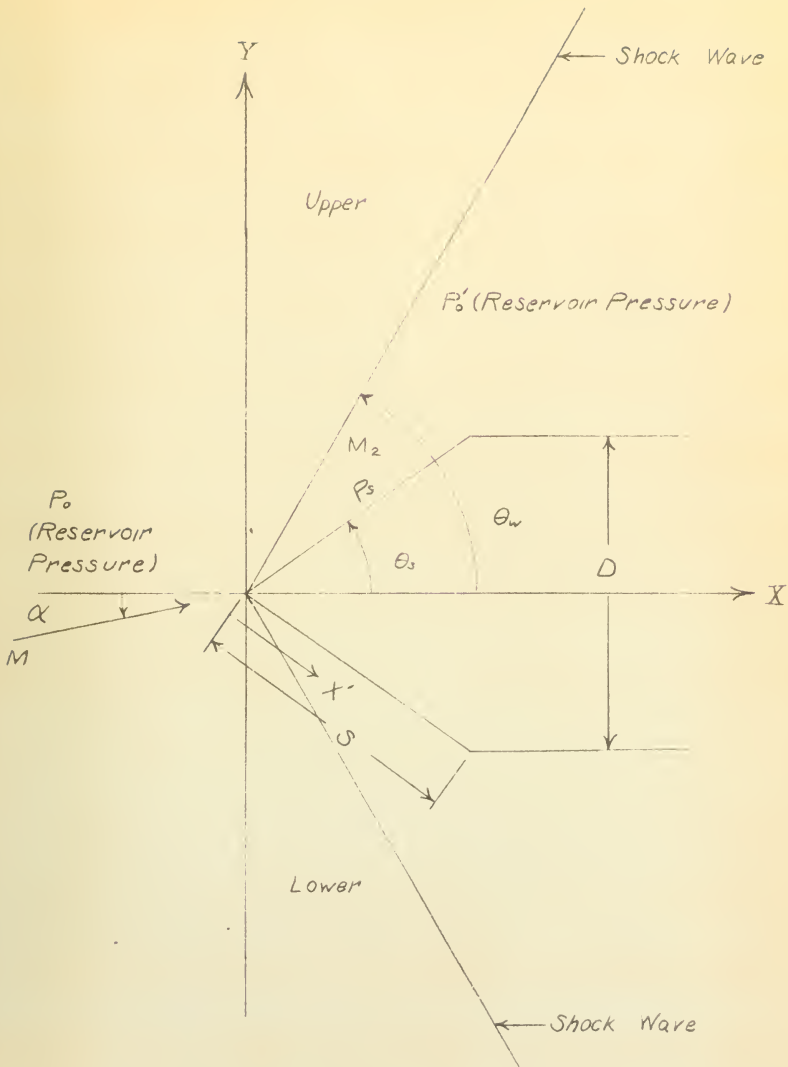


FIG. 3
 $M = 1.438$
 LOWER

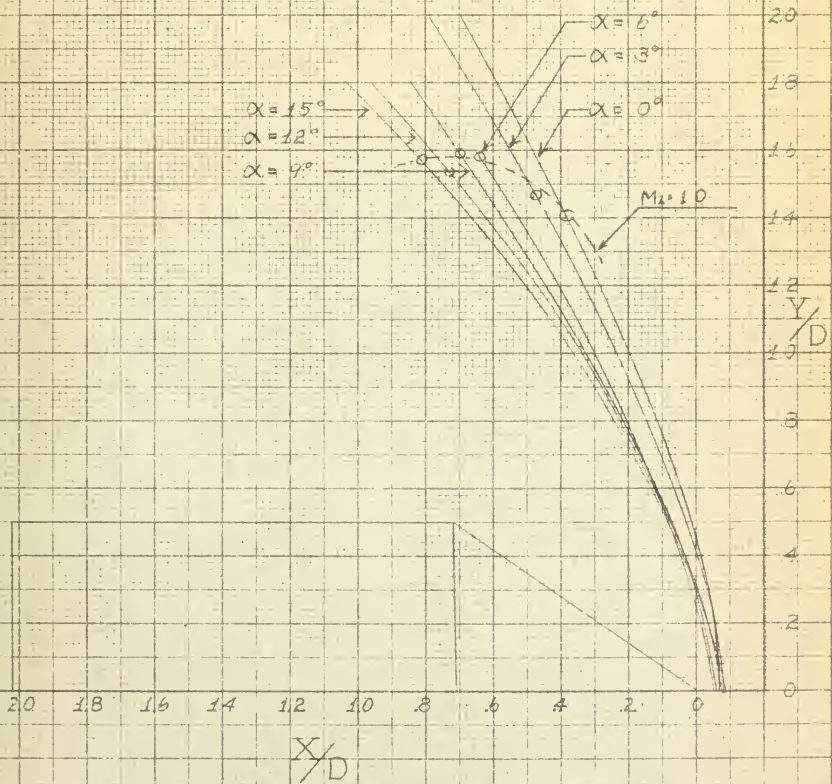


FIG 4
 $M = 1.438$
 UPPER

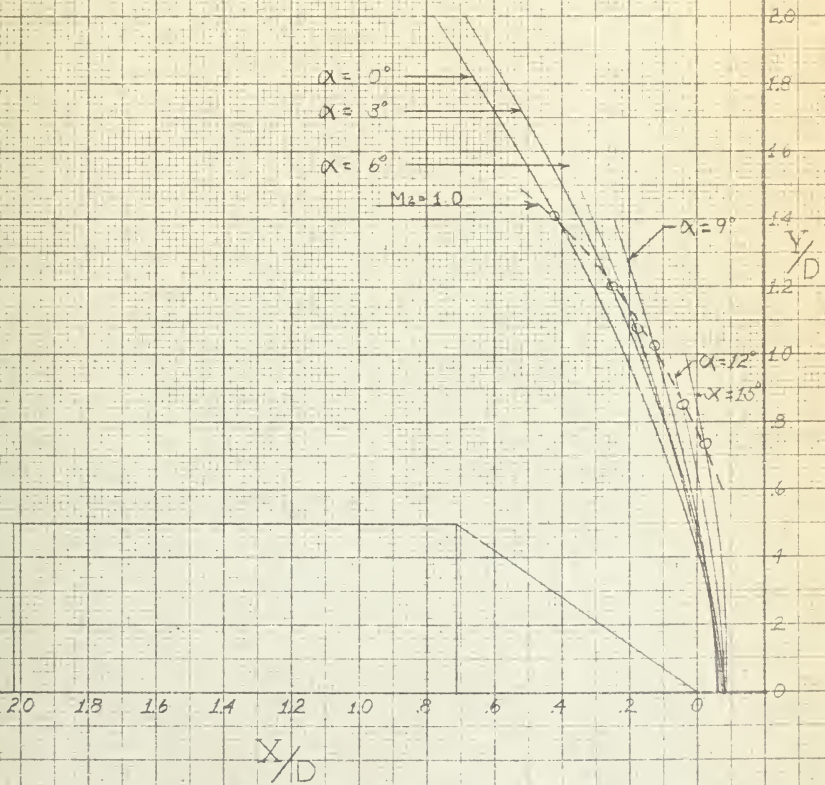


FIG 5
M = 1.544
LOWER

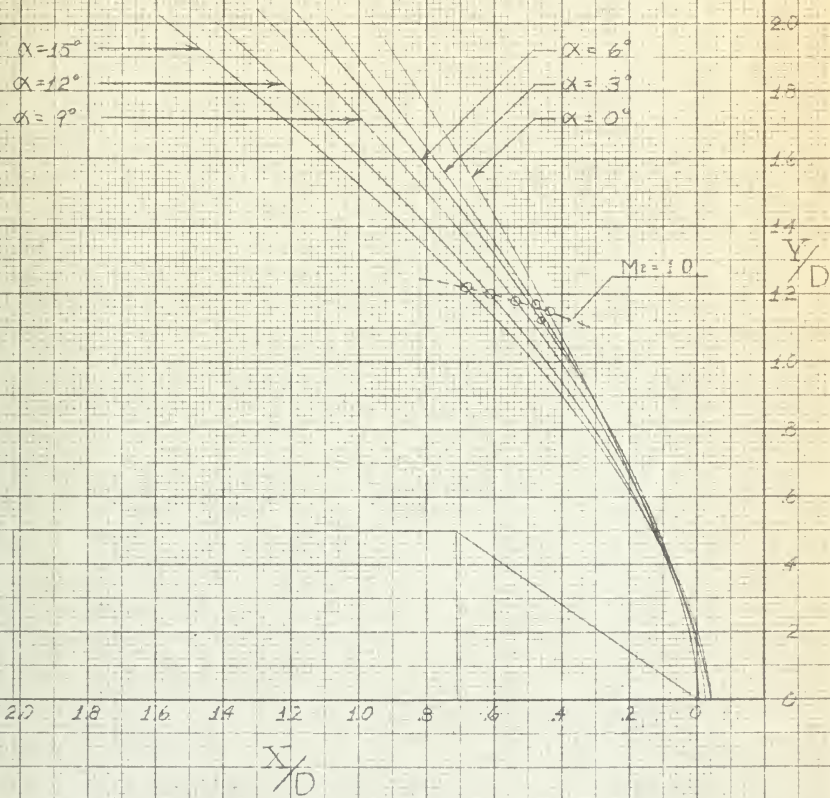


FIG. 6
 $M = 1.544$
 UPPER

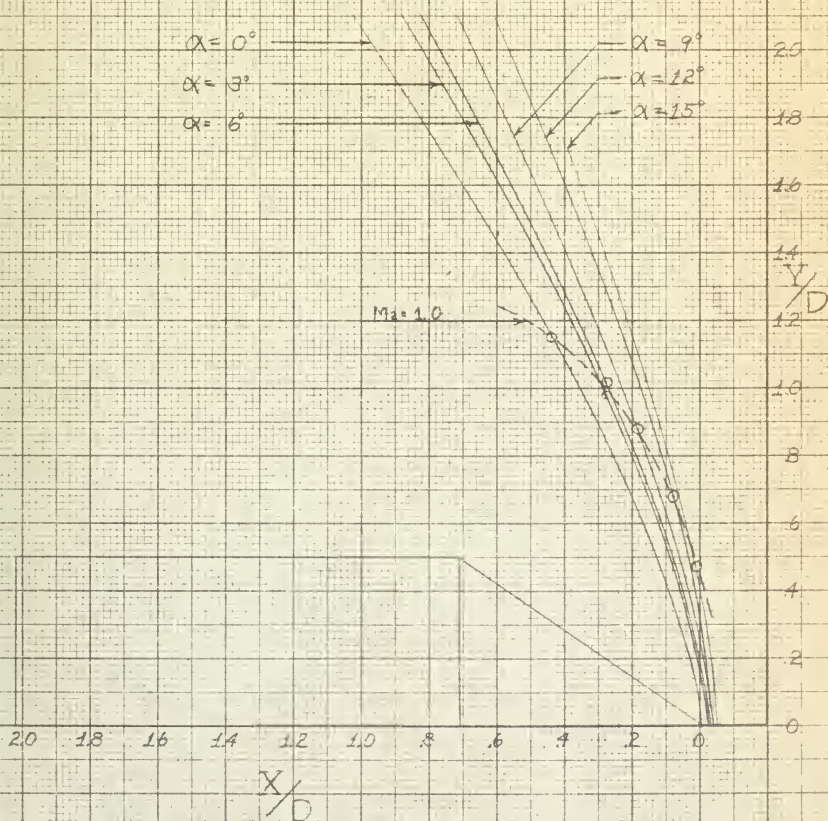


FIG. 7
M = 1.584
LOWER

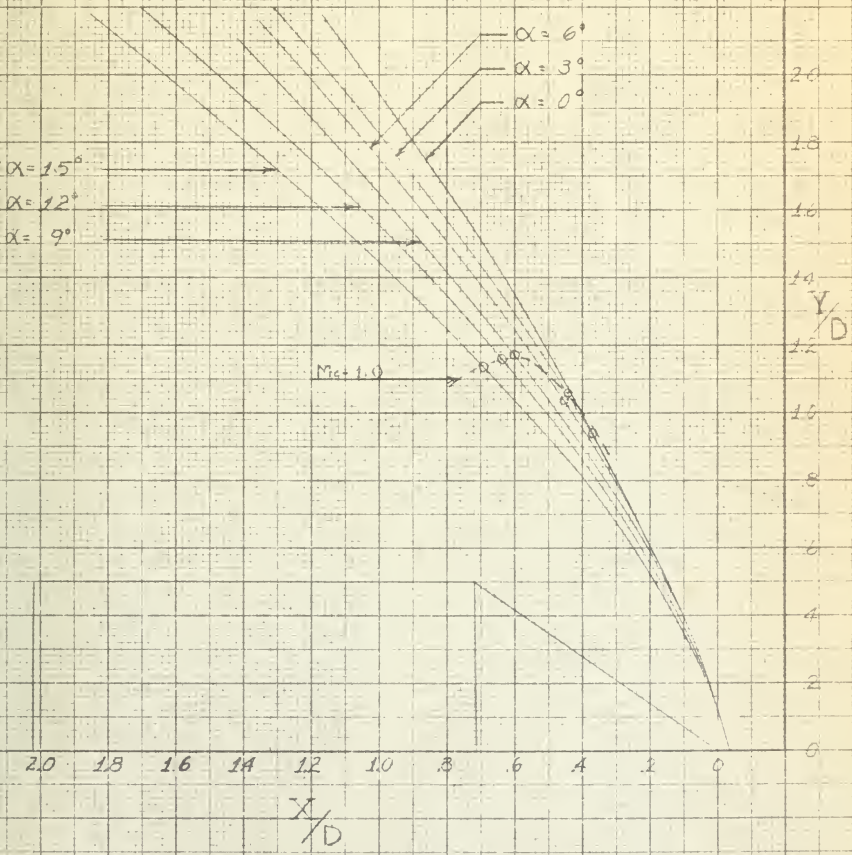


FIG 8
M = 1.584
UPPER

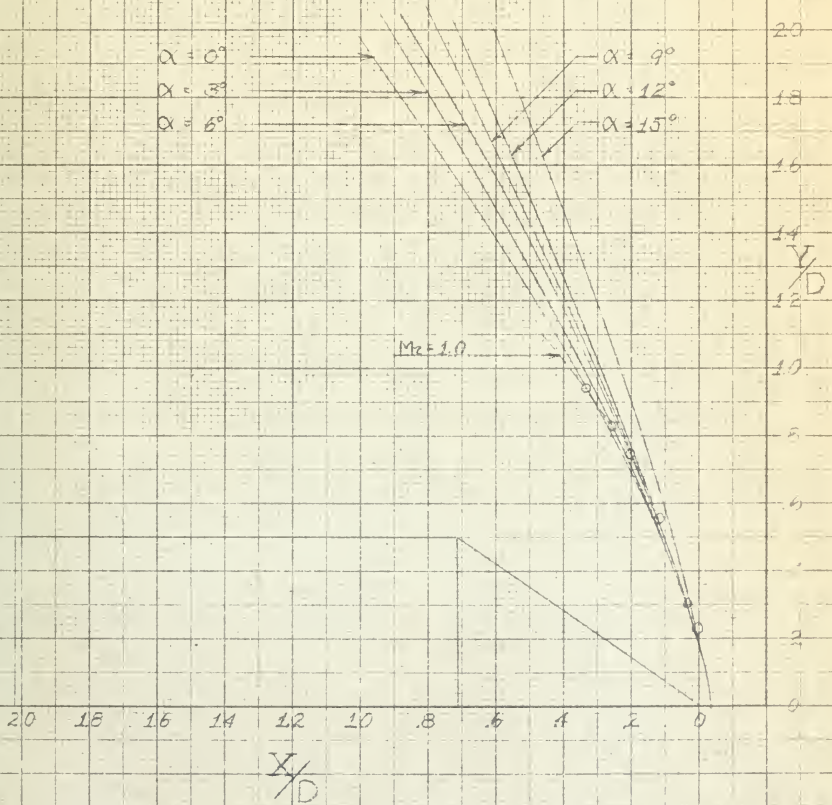


FIG. 9
M = 1.857
LOWER

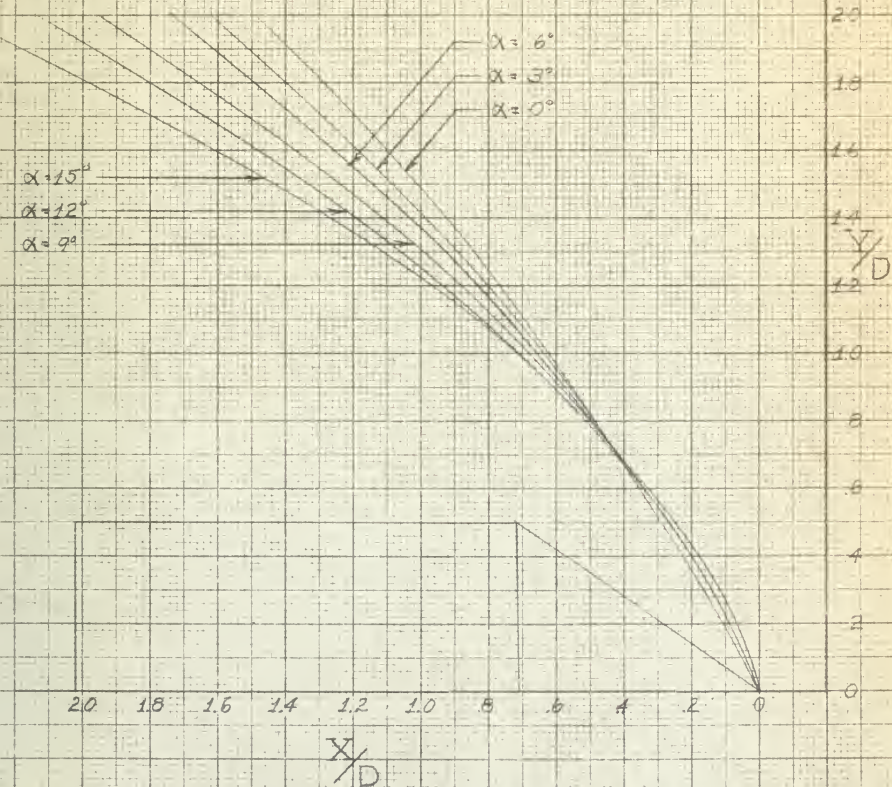


FIG 10
 $M = 1857$
 UPPER

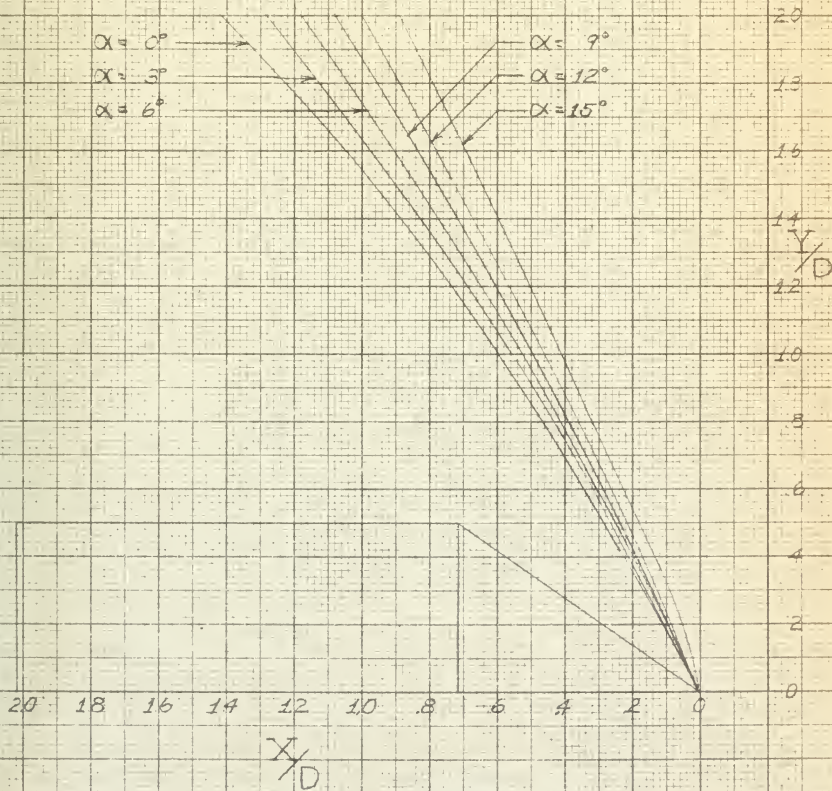


FIG. 11
M = 1.986
LOWER

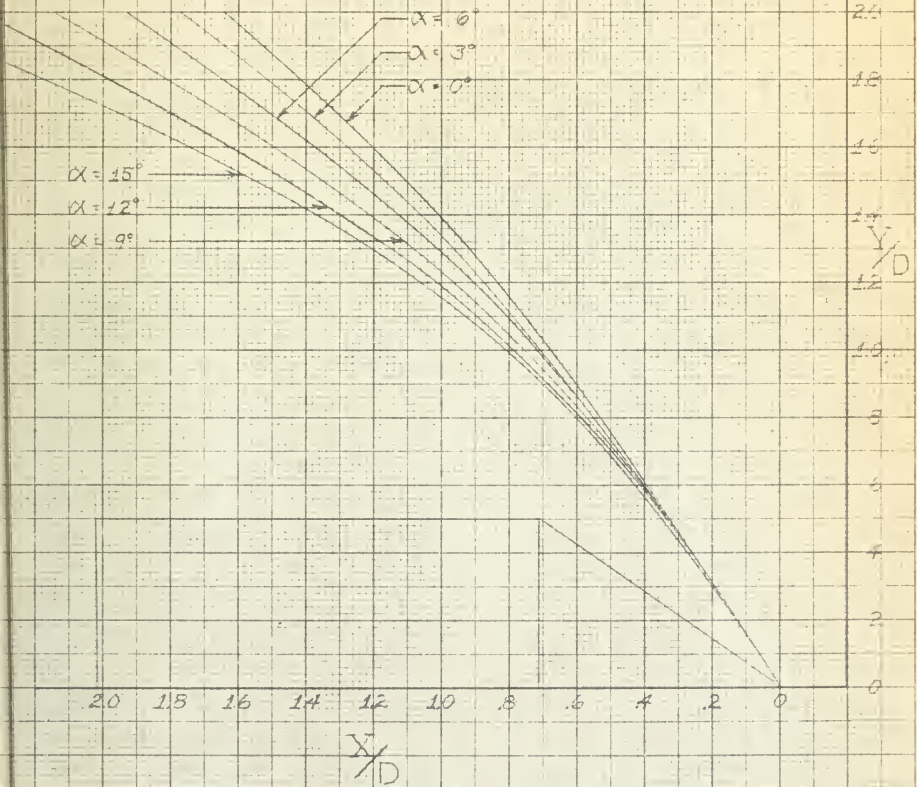


FIG 12
 $M = 1.986$
 UPPER

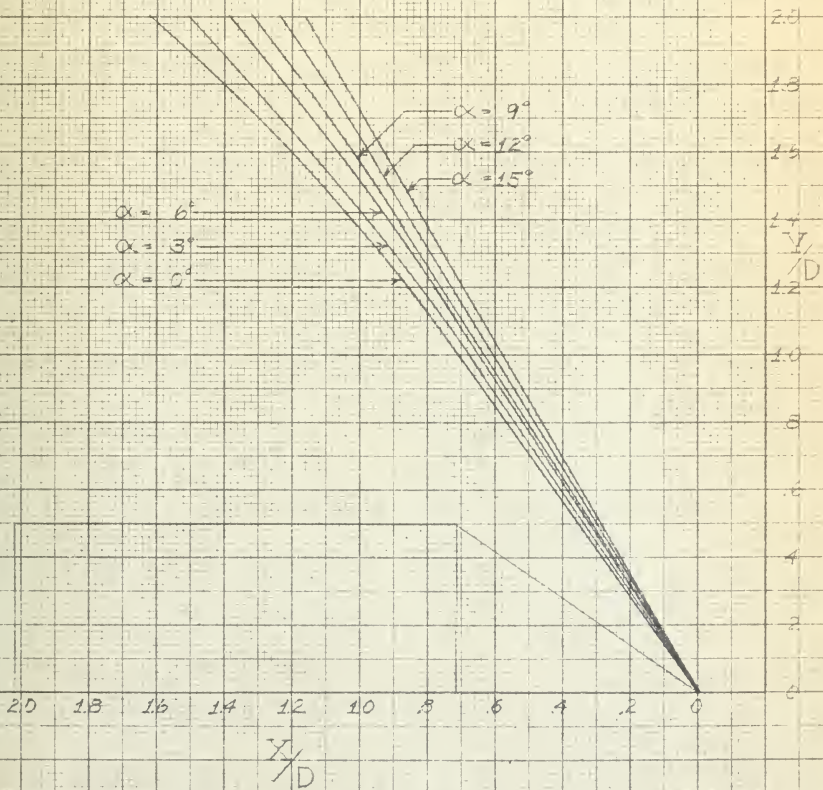


FIG 13
 $M = 3.01$
 LOWER

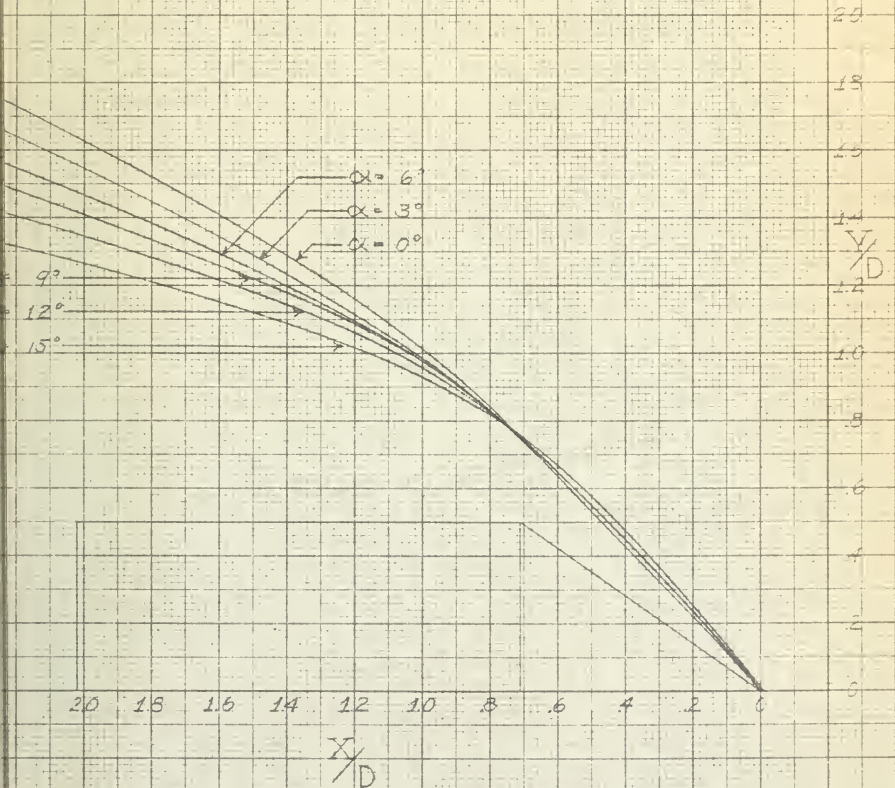


FIG 14
 $M=3.01$
 UPPER

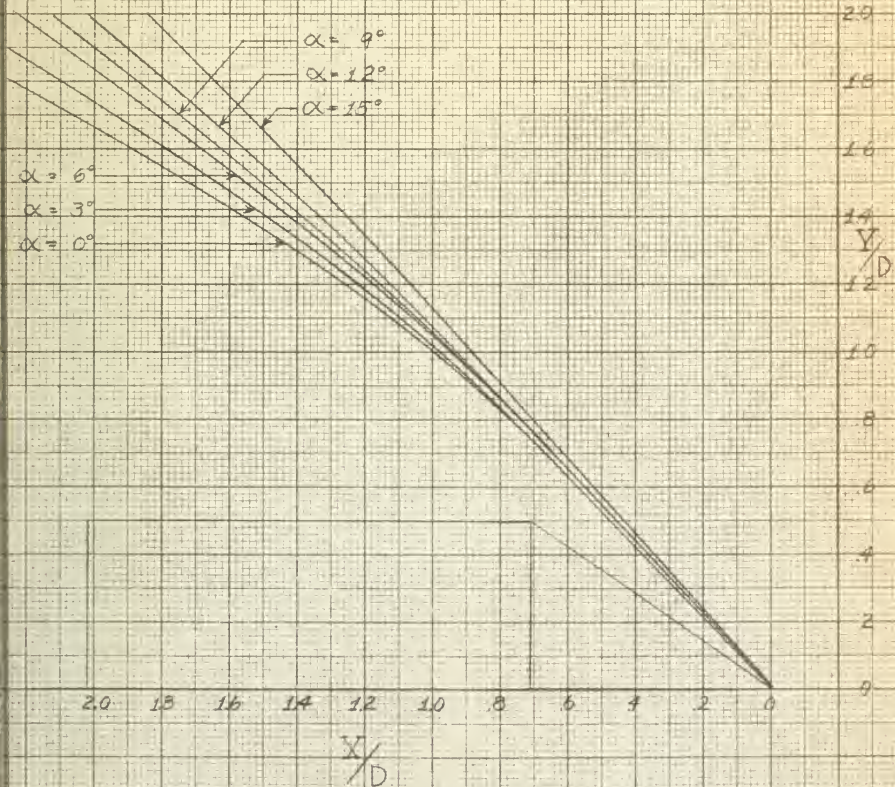


FIG 15
 $\alpha = 0^\circ$
 UPPER AND LOWER

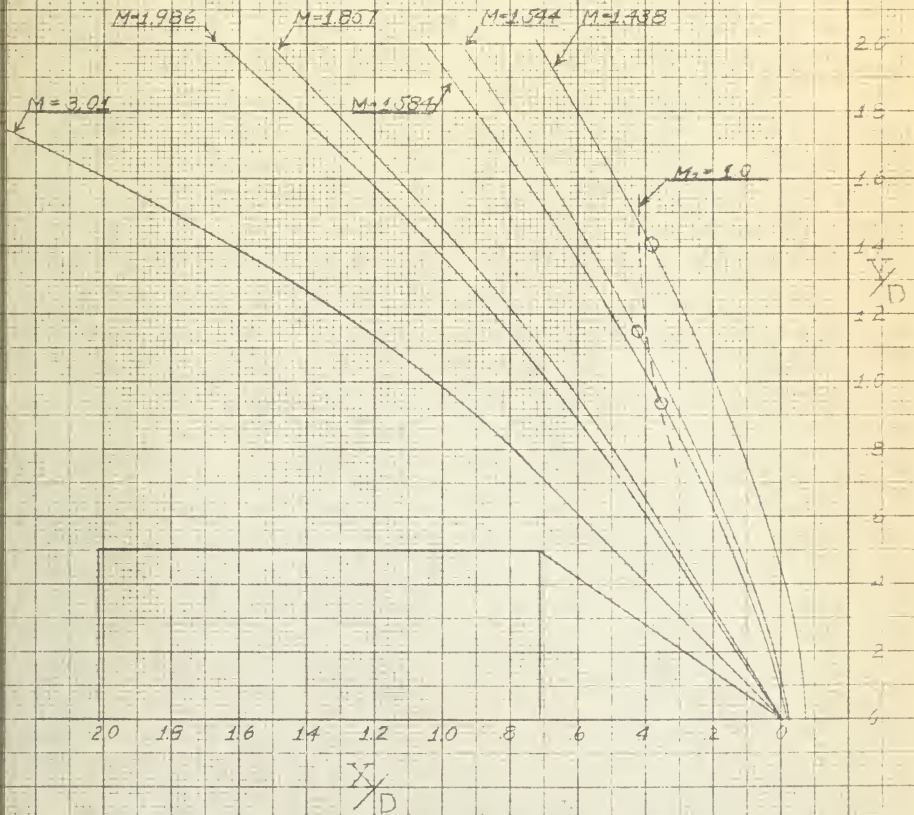


FIG 16
 $\alpha = 3^\circ$
LOWER

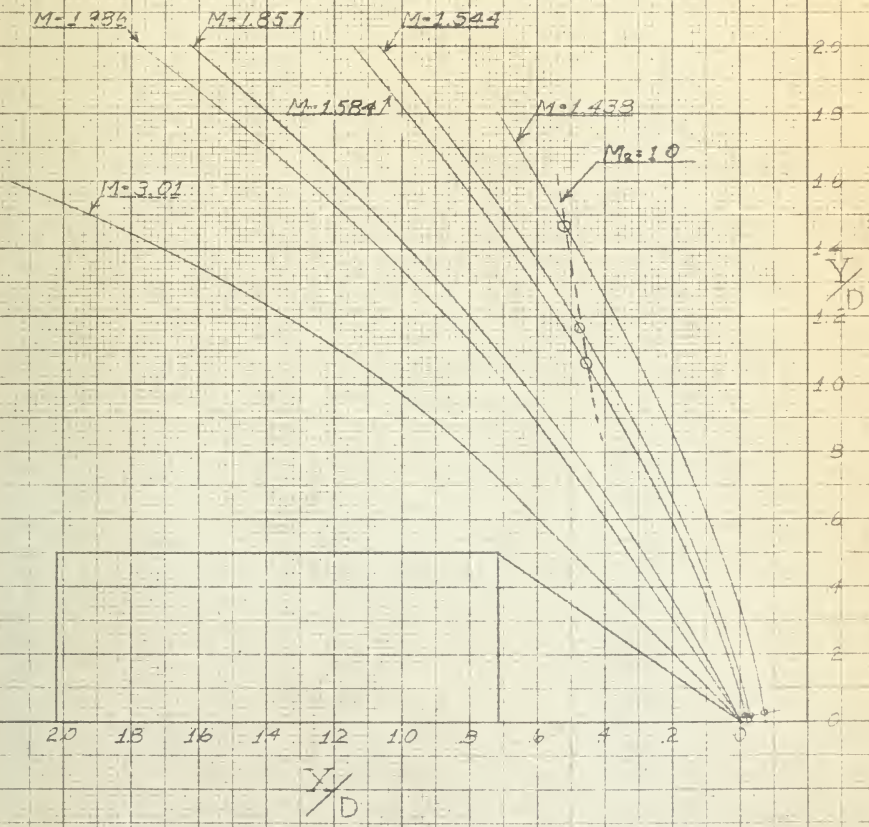


FIG. 17
 $\alpha = 3^\circ$
UPPER

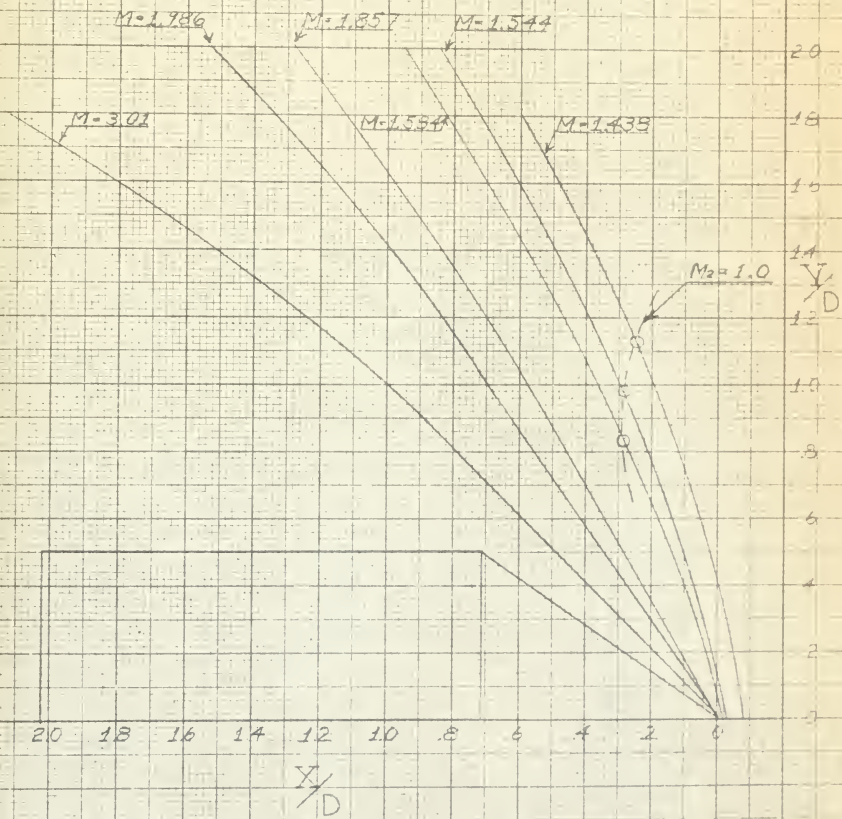


FIG 18
 $\alpha = 6^\circ$
 LOWER

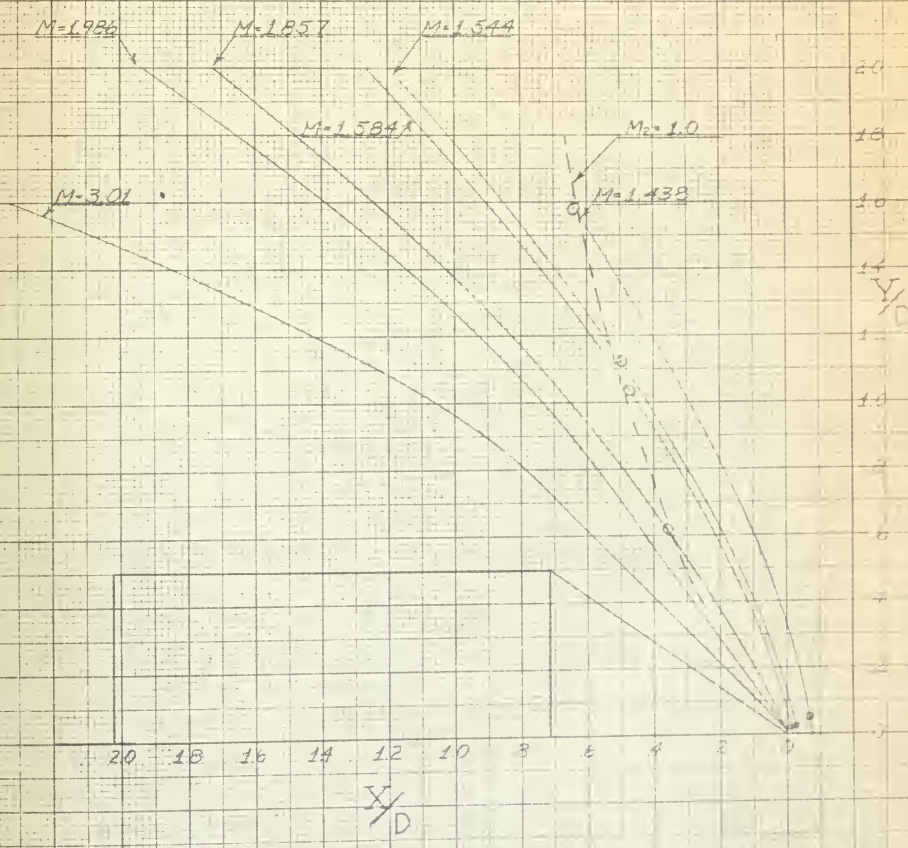


FIG 19

$\alpha = 6^\circ$

UPPER

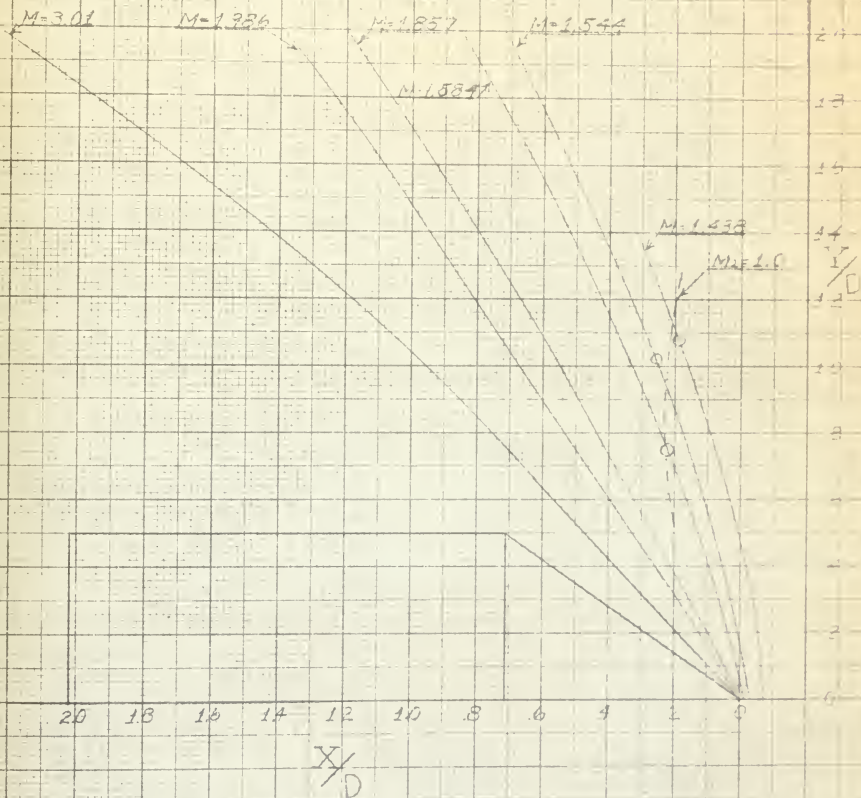


FIG 20

$\alpha = 9^\circ$

LOWER

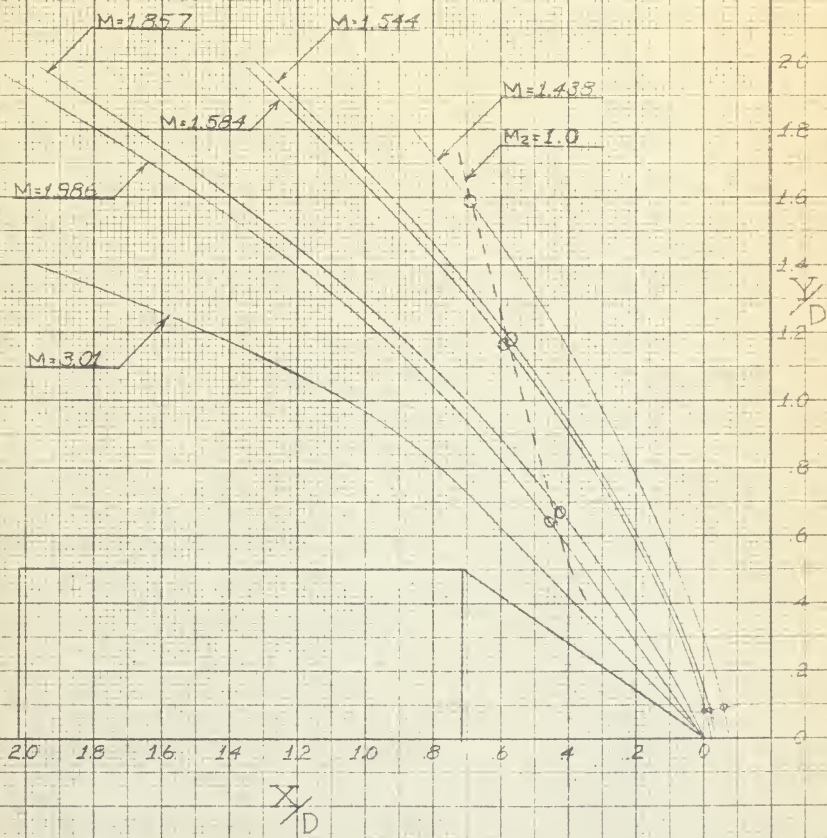


FIG 21
 $\alpha = 9^\circ$
 UPPER

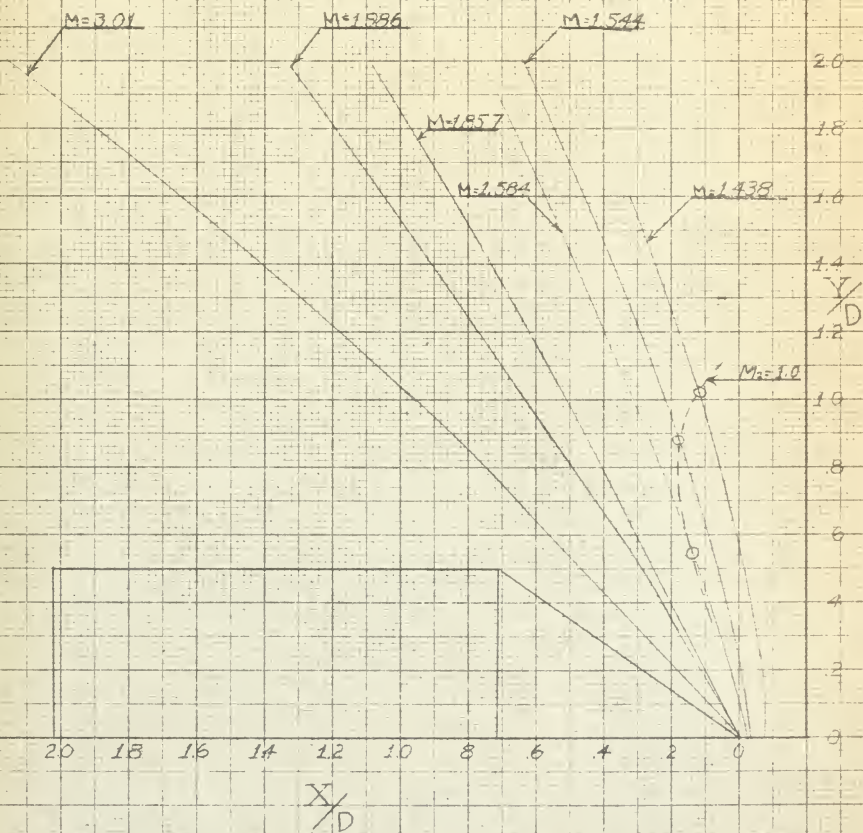


FIG 22
 $\alpha = 12^\circ$
 LOWER

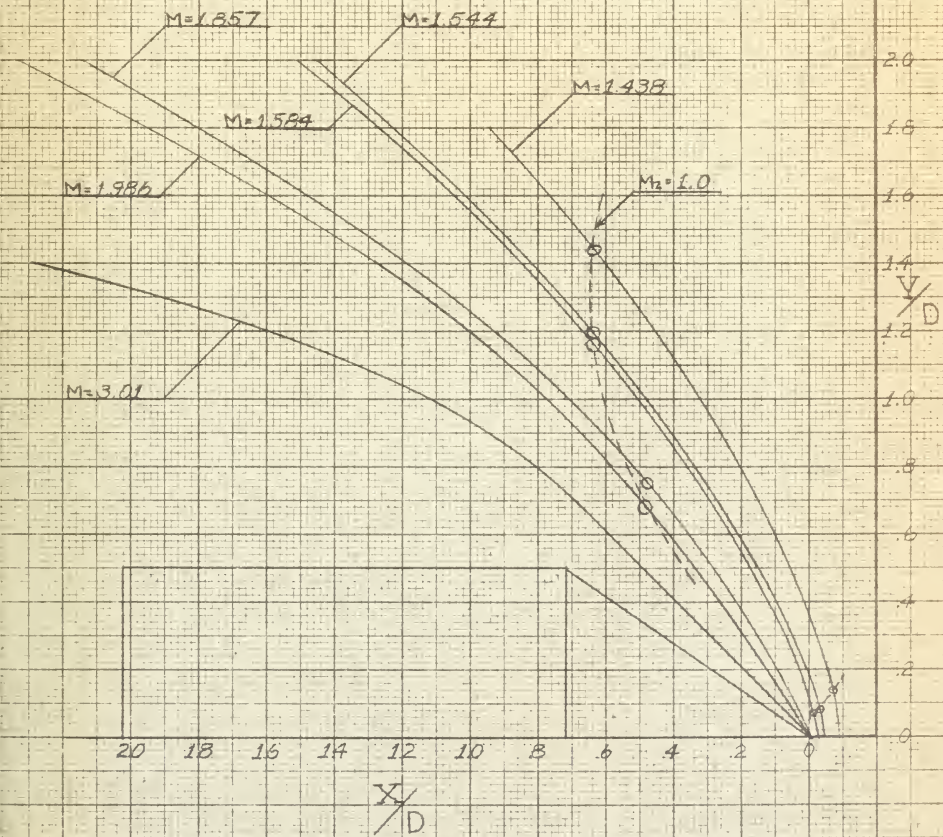


FIG 23

 $\alpha = 12^\circ$

UPPER

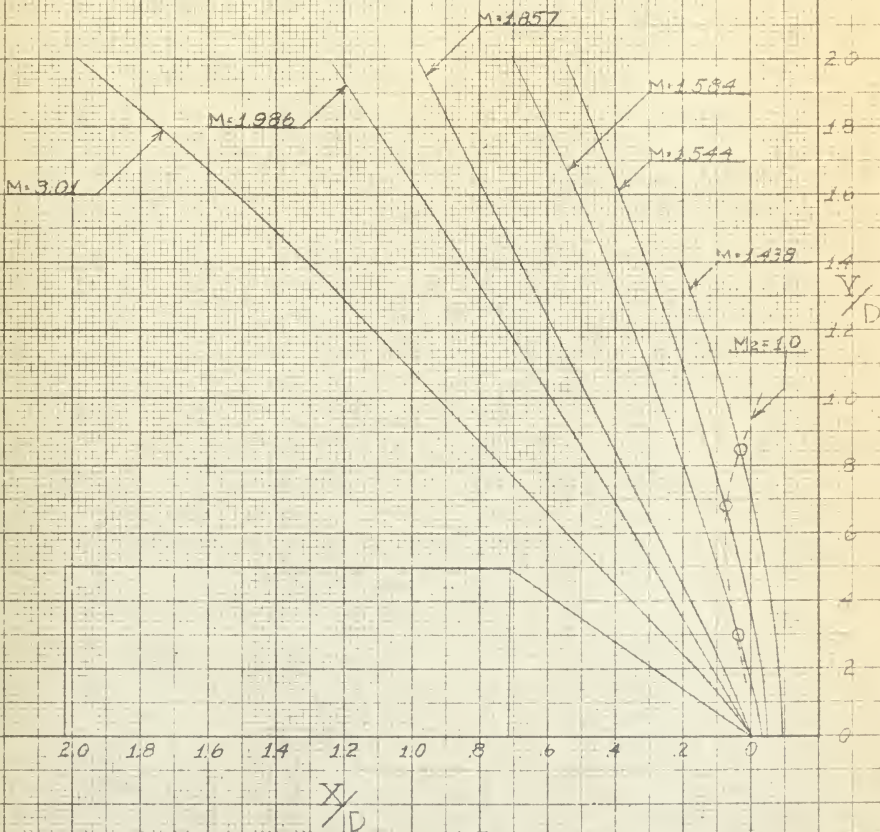


FIG 24
 $\alpha = 15^\circ$
 LOWER

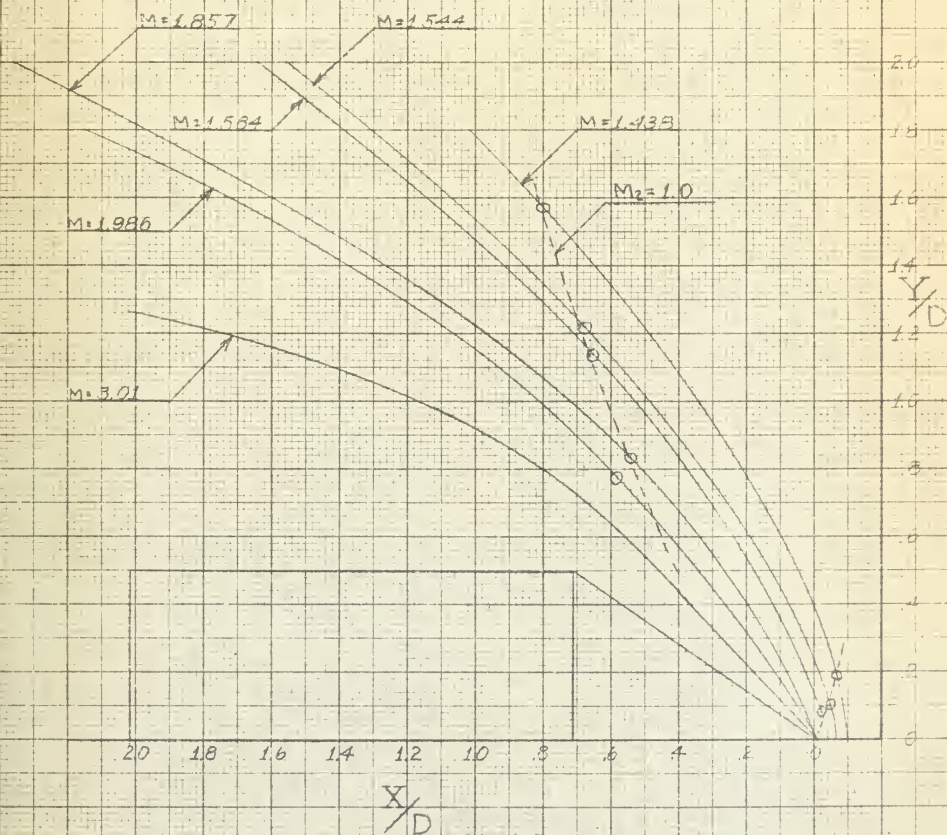


FIG. 25
 $\alpha = 15^\circ$
 UPPER

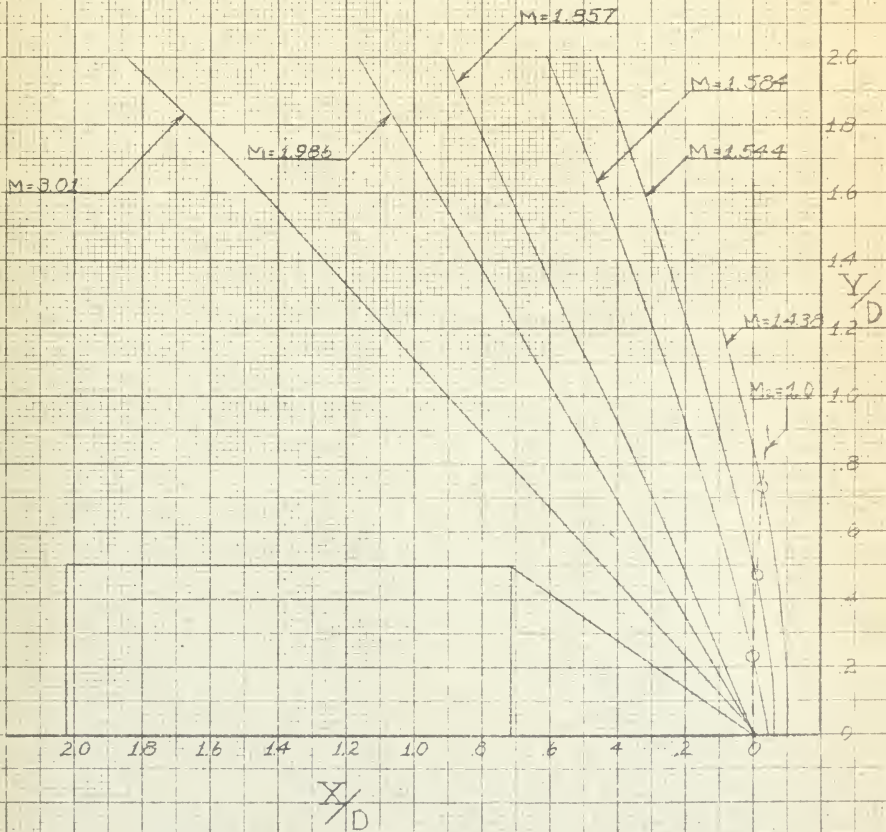


FIG. 26
 MAXIMUM FLOW DEFLECTION
 (TAYLOR-MACCOLL THEORY)

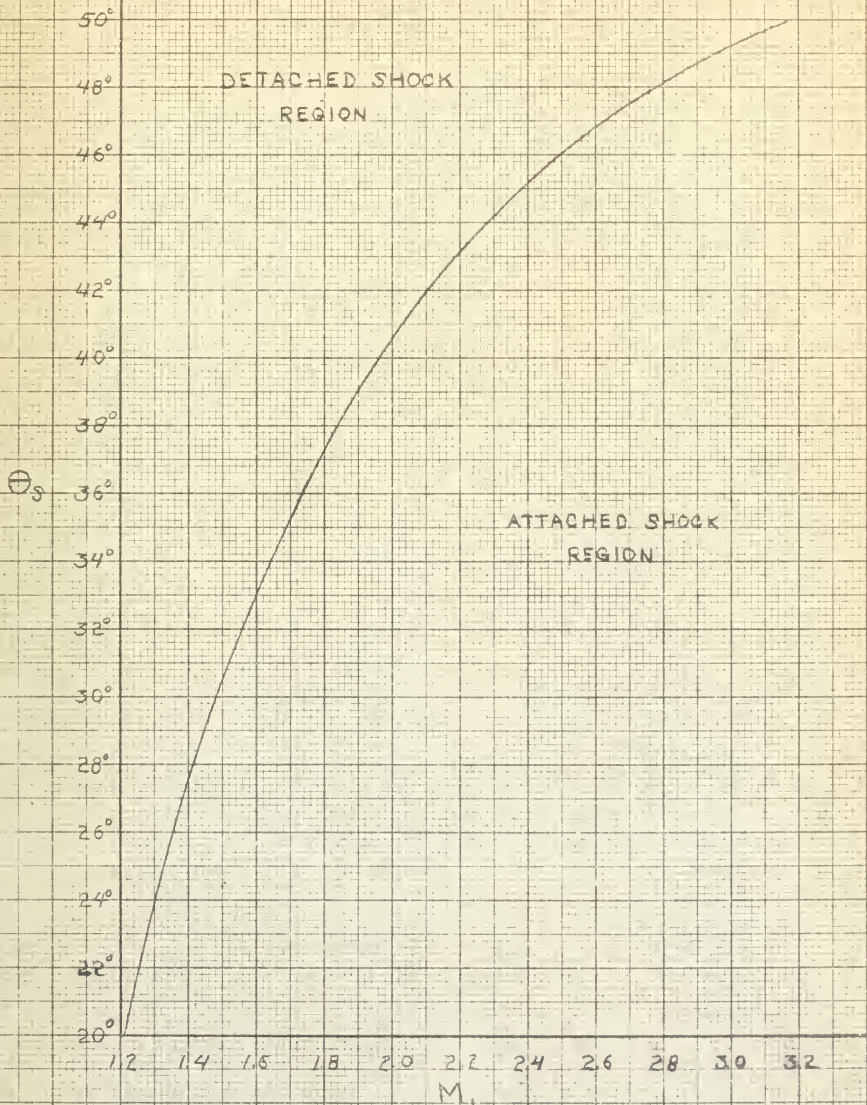


FIG. 27
 SURFACE PRESSURE DISTRIBUTION
 $M = 1.584$

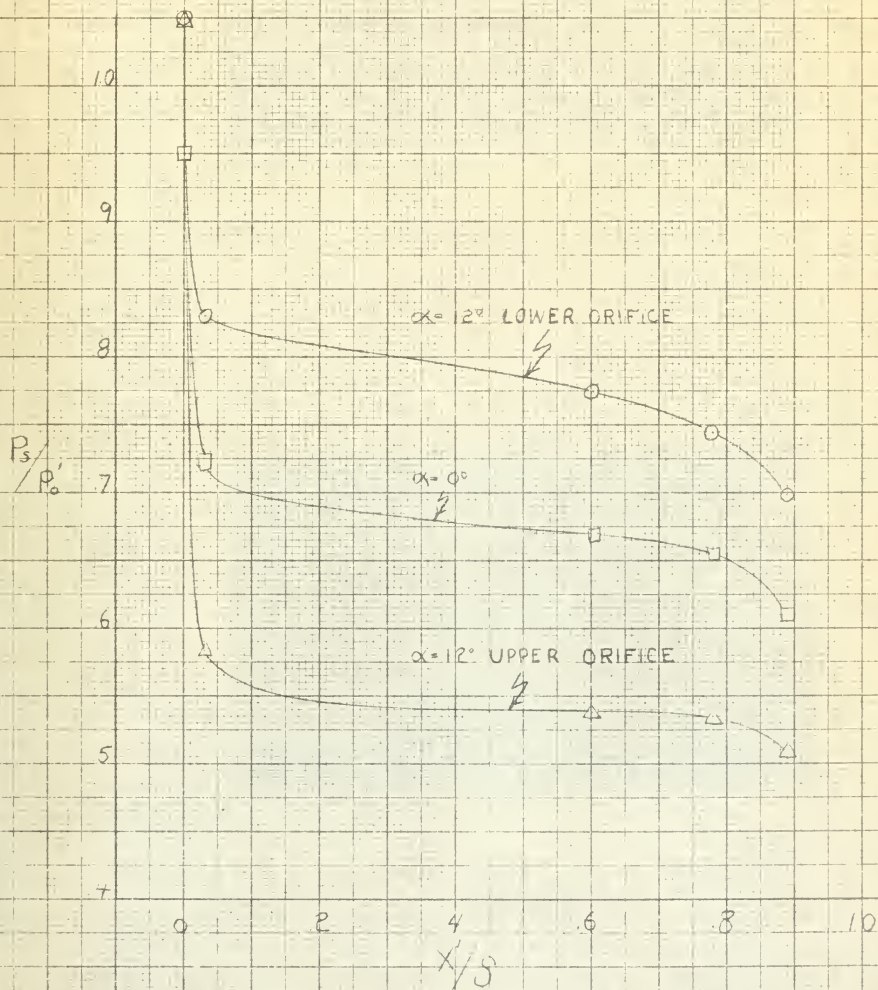




Fig. 28
 $M = 1.544$
 $\alpha = 0^\circ$



Fig. 29
 $M = 1.544$
 $\alpha = 15^\circ$



Fig. 30
 $M = 1.584$
 $\alpha = 0^\circ$



Fig. 31
 $M = 1.584$
 $\alpha = 15^\circ$



Fig. 32
 $M = 1.857$
 $\alpha = 0^\circ$



Fig. 33
 $M = 1.857$
 $\alpha = 15^\circ$

9 SEP 70

19324

Thesis

12994

The
F88

F88

Frick

Experimental investi-
gation of detached shock
waves on a 70° cone...

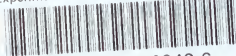
Exp
sho

9 SEP 70

19324

thesF88

Experimental investigation of detached s



3 2768 001 90042 6

DUDLEY KNOX LIBRARY